Advanced Catalytic Technologies for Compressed Natural Gas–Gasoline Fuelled Engines

Wahbi, Ammar; Tsolakis, Athanasios; Herreros, Martin; Zeraati Rezaei, Soheil; Doustdar, Omid; Millington, P. J.; Raj, A.

DOI:
10.1595/205651323X16669674224875

https://doi.org/10.1595/205651323X16669674224875 *Johnson Matthey Technol. Rev.*, 2023, **67**, (2), 171–185

JOHNSON MATTHEY
TECHNOLOGY REVIEW

technology.matthey.com

Advanced Catalytic Technologies for Compressed Natural Gas–Gasoline Fuelled Engines

Challenges in methane abatement

A. Wahbi, A. Tsolakis*, J. M. Herreros, S. Zeraati-Rezaei, O. Doustdar
Mechanical Engineering, The University of Birmingham, Edgbaston, Birmingham, B15 2TT, UK

P. J. Millington, A. Raj
Johnson Matthey, Blounts Court, Sonning Common, Reading, RG4 9NH, UK

***Email:** A.Tsolakis@bham.ac.uk

PEER REVIEWED

Received 7th July 2022; Revised 24th October 2022; Accepted 25th October 2022; Online 31st October 2022

The main challenges of compressed natural gas (CNG) engine fuelling in terms of methane abatement in the aftertreatment system are addressed in this study using differently loaded platinum group metal (pgm) catalysts. A dual-fuel injection strategy of methane-gasoline was implemented where methane gas was port-injected into the intake in stoichiometric conditions at levels corresponding to 20% and 40% energy density replacement of gasoline fuel. High, medium and low loaded palladium-rhodium catalysts were used and compared to study the effect of pgm loading on the catalyst light-off activity for methane. Results indicate that increasing the palladium loading led to significantly earlier light-off temperatures achieved at relatively lower temperatures of 340°C, 350°C and 395°C respectively. However, the benefit diminishes above palladium loading >142.5 g ft^{-3}. The study has also demonstrated that ammonia is formed over the CNG catalyst due to steam-reforming reactions from the increased levels of methane in the exhaust with dual-fuelling. Hence aftertreatment technologies such as selective catalytic reduction (SCR) should be adopted to remove them. This further highlights the need to regulate the harmful ammonia emissions from future passenger cars fuelled with CNG. In addition, the benefits of the dual-fuel system in terms of lower engine output carbon dioxide, non-methane hydrocarbon (NMHC) and particulate matter (PM) emissions compared to the gasoline direct injection (GDI) mode alone are presented.

1. Introduction

CNG is currently a promising and relatively well established alternative to conventional liquid fossil fuels. The increased interest in methane-based fuels such as biogas, biomethane and natural gas is mainly driven by increasingly tight exhaust-emission standards being imposed as they produce comparatively lower CO_2 and PM emissions during combustion than petroleum based internal combustion engines (1–3). Moreover, large proven reserves of natural gas and its lower price compared to petroleum have also driven market demand. However, CNG fuelled internal combustion engines suffer power losses of over 10% compared to the same size gasoline engines. This is because CNG replaces a larger volume of air in the intake, resulting in lower volumetric efficiencies (2). As such, a dual-fuel mode which combines the advantages of CNG and gasoline fuels in terms

of lower exhaust emissions and better engine performance in spark-ignition (SI) engines has been investigated (3–8).

The synergies of CNG and gasoline fuel in SI engines can lead to lower fuel consumption and lower exhaust emissions. Obiols *et al*. (5) investigated the injection of gasoline and CNG on a 1.6 l turbocharged GDI engine with an independent CNG port-injection system. Their results showed that a trade-off point between performance, fuel consumption and exhaust emissions can be reached for a gasoline mass fraction of about 40%. Concerning the engine-out exhaust emissions, CNG engines generally produce lower carbon monoxide emissions and unburned NMHC than naturally aspirated gasoline engines (1, 2). However, CNG engines produce large concentrations of methane, which is a greenhouse gas (30 times the effect of CO_2 over 100 years). The exhaust gasses produced from a SI engine depend drastically on the air-fuel ratio (λ), also expressed as the equivalence ratio (φ). In a CNG fuelled SI engine running at stoichiometric conditions (λ = 1), a three-way catalyst (TWC) is used to effectively reduce carbon monoxide, nitrogen oxides (NOx) and hydrocarbons (HCs). However, methane is highly difficult to oxidise in a TWC (>500°C) due to the high stability of its C–H bond (9). Therefore, catalysts adapted for improving methane oxidation will need to be employed in CNG fuelled engines. In that context, no study to date has investigated the performance of the aftertreatment system designed for dual-fuel gasoline-CNG engines, with all studies either limited to combustion analysis of the dual-fuel or for dedicated CNG fuelled engines.

The performance of a palladium-rhodium TWC on the exhaust emissions of a standard gasoline engine fuelled with CNG has been studied (10). Results showed that exhaust emissions from a CNG fuelled engine behave similarly to standard gasoline engines. The effect of the engine's lambda is apparent where carbon monoxide emissions are completely depleted at stoichiometric and lean conditions, while NOx and HC conversions reach up to 100% and 95% just rich of stoichiometry respectively, before drastically decreasing at lean conditions. They suggest an increase in pgm loading will lead to an improvement in HC conversions under stoichiometric conditions due to the significantly high light-off temperature of methane, which is the main constituent of total hydrocarbon (THC) emissions from CNG engines. Lehtoranta *et al*. (9) investigated the effect of a combined system consisting of a SCR and a methane oxidation catalyst with urea injection on the exhaust emissions of a CNG fuelled gasoline engine. The combined system was able to reduce NOx and methane emissions by up to 95% and 50% respectively at ~400°C. However, such systems are expensive and rather complicated due to the need for careful control of urea injection in addition to urea storage problems.

As such, the main aim of this work is to fill the literature gap in the aftertreatment system of dual-fuel engines by investigating the effect of real engine exhaust gas on the performance of CNG catalysts especially in reducing methane emissions, under different fuelling compositions. The dual-fuel injection of methane-gasoline provides an alternative solution for vehicle manufacturers to meet future emission targets, possibly using only a CNG catalyst. If advantageous results are yielded by this study, then the potential for further aftertreatment development for test cycles corresponding to the Worldwide Harmonised Light Vehicle Test Procedure (WLTP) and Real Driving Emissions (RDE) should be considered.

2. Experimental Setup and Methodology

2.1 Engine Test Bench

In this study, a 1.5 l, three-cylinder, turbocharged research gasoline engine was used. A schematic view of the engine and test apparatus is shown in **Figure 1**. The engine can be run with dual injection mode, direct injection (DI) and port fuel injection of gasoline fuel, although only DI mode was used in this study. **Table I** summarises the basic engine specification.

2.2 Experimental Procedure

The engine was operated at idle conditions for 20 min to reach operational coolant and oil temperatures of 90 ± 1°C and 95 ± 2°C respectively, to avoid cold-start effects and minimise emission fluctuation. Tests were carried out at a steady-state condition with a fixed engine speed of 2100 ± 2 rpm and a load of 30 ± 2 Nm, corresponding to a low load condition for vehicles.

The level of gasoline energy density (ED) replacement by methane was conducted at three conditions: 0, 20% and 40% replacement. The conditions, for differentiation purposes, are denoted as 'M0', 'M20' and 'M40', respectively. The maximum replacement level, M40, was selected as

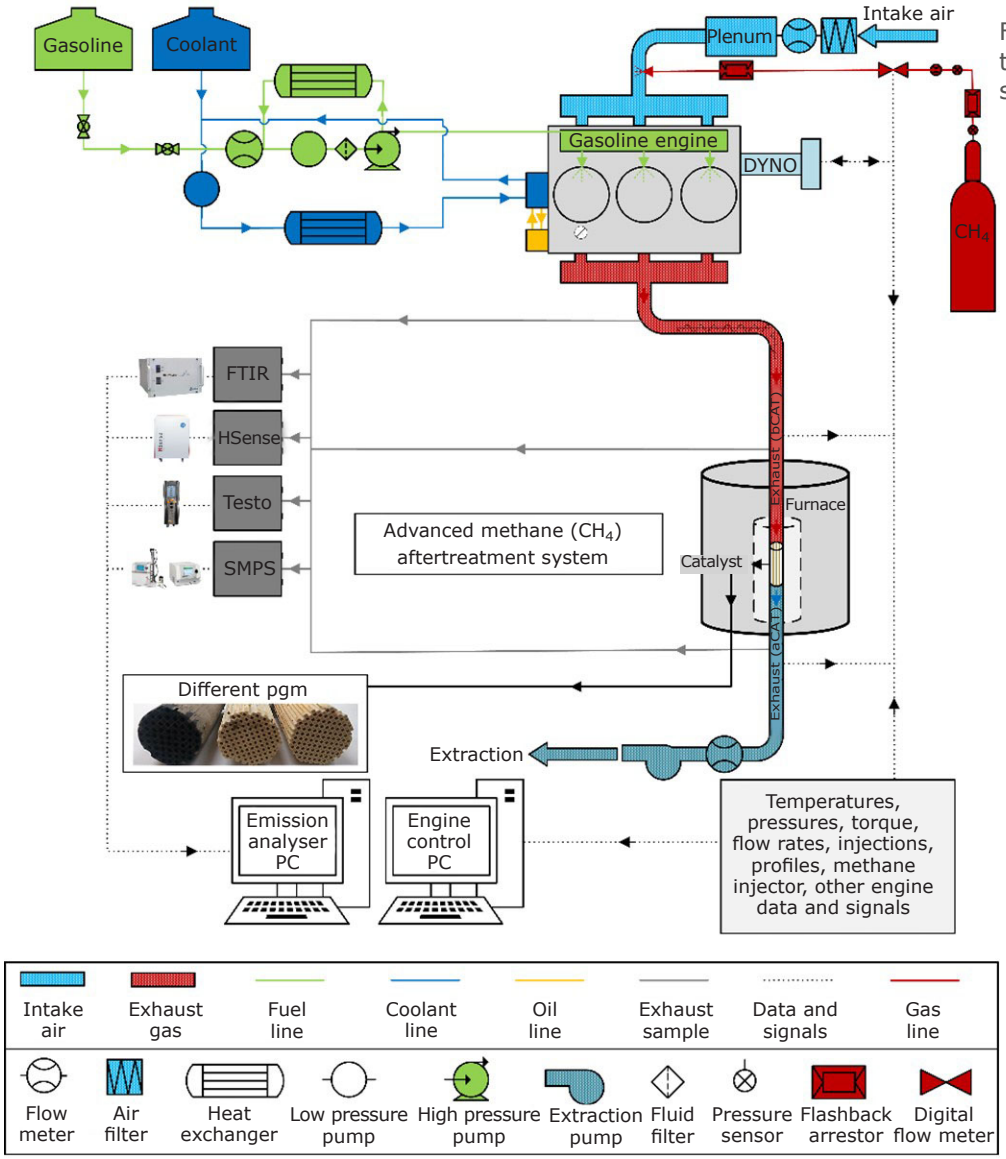

Fig. 1. Engine apparatus, testing and analysis schematic

Table I Gasoline Direct Injection Engine Specifications and Associated Apparatus

Engine type	**Spark-ignition, three-cylinder**
Charged method	Turbocharged
Compression ratio	11:1
Swept volume	1497 cc
Number of cylinders	3
Rated power	134 kW at 6000 rpm engine speed
Rated torque	240 Nm at 1600–4500 rpm engine speed

it provides a good balance between avoiding start-up issues and poorer performance associated with methane fuelling, and a large enough proportion of methane to yield the particulate reduction benefits of the fuel. Methane gas was port-injected into the engine cylinder and the spark timing was adjusted in order to phase the mass fuel burn 50% (MFB50%) of the dual-fuel to that of the baseline gasoline. This was done to evaluate the effect of methane addition, in isolation, on the emitted gaseous and particulate emissions. The in-cylinder air:fuel (A:F) ratios were controlled at stoichiometric conditions for all cases. Temperature and flowrate of methane gas were monitored throughout the experiment to ensure there were no drastic changes in density that would invalidate the replacement ratio. The replacement accuracy control can be considered as 3%.

Table II details the contrasting fuel properties of the gasoline and methane gas used. The engine operates with standard EN228 gasoline containing 5% (v/v) ethanol content supplied by Shell, UK,

Table II Fuel Properties for Gasoline and Methane Gas

	Gasoline	Methane gas
C:H ratio	6.20	0.25
Calorific value, MJ kg^{-1}	41.65	50
Research octane number	95.8	>120
Density @ 15°C, kg m^{-3}	746.6	0.671

and 99.95% methane gas (representative of CNG) supplied by BOC, UK.

3. Results and Discussion

3.1 Combustion Studies

To allow for impartial comparisons to be made between the engine-out emissions of the different fuelling compositions, the spark timing was adjusted in order to phase the combustion and keep the MFB50% identical. The slower laminar flame speed velocity of methane gas promotes a slower flame propagation rate leading to a longer combustion duration compared to the gasoline mode. Thus, the spark timing was slightly advanced when the methane proportion was increased with respect to only gasoline operation to achieve equal MFB50%. As a result of phasing the combustion, the maximum in-cylinder pressure (P_{max}) with methane replacement was identical to that of the baseline gasoline mode, while the heat release rate (HRR) reduced with the addition of methane to the combustion chamber as seen in **Figure 2**. Combustion started earlier with M20 and M40 and the prolonged compression stroke resulted in higher in-cylinder temperature, as demonstrated in the HRR profile. Moreover, the engine combustion improved with the addition of methane as evidenced by the decrease in the coefficient of variance (COV) of the indicated mean effective pressure (IMEP), shown in **Table III**. The addition of gaseous methane improved the homogeneity of the air-fuel mixture and reduced the impact of poor liquid fuel evaporation under low load conditions and thus promoted a more stable combustion (10).

Table III details the brake specific fuel consumption, thermal efficiency, COV of IMEP and engine exhaust temperatures of the studied fuel compositions. The addition of 20% methane reduced the brake specific fuel consumption by 4.5% compared to the baseline gasoline-mode due to the higher mass-based heating value of methane. In comparison, the addition of 40% methane led to a 5.3% reduction in fuel consumption (6). This is also highlighted by the increase in thermal efficiency of the engine with the addition of methane, as detailed in **Table III**. Further optimisation of spark timing for natural gas operation can lead to even higher improvements in terms of fuel consumption. The higher-octane quality of natural gas reduces the knock intensity of the engine, thus enabling the spark timing to be more advanced and the combustion phasing maintained close to peak efficiency. This would be particularly beneficial at higher loads eliminating the need for fuel enrichment (running rich of

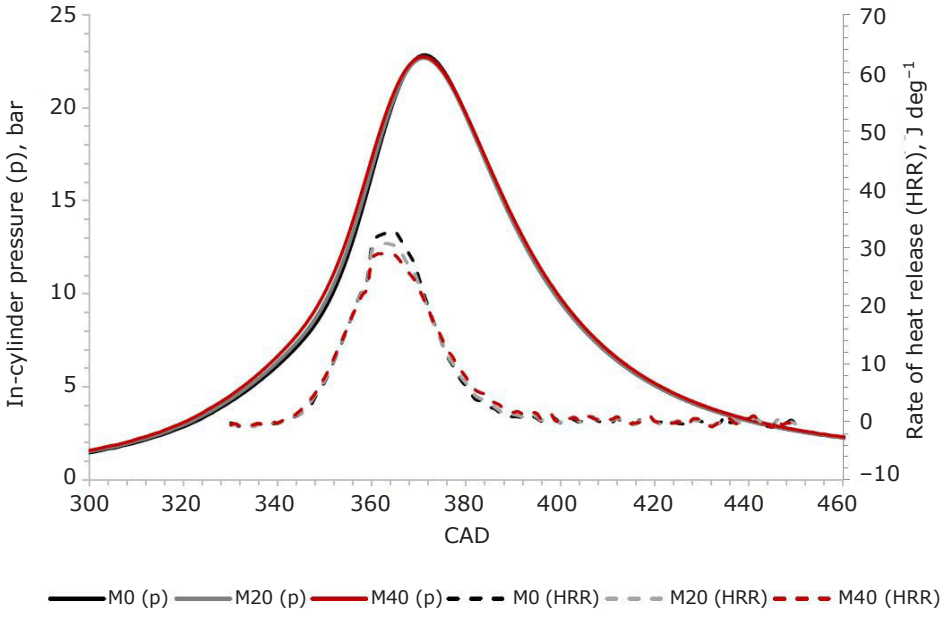

Fig. 2. In-cylinder pressure trace and rate of heat release for each fuelling condition

Table III Engine Parameters for the Different Compressed Natural Gas Replacements

Methane replacement, %	Brake specific fuel consumption, g kWh^{-1}	Thermal efficiency, %	Coefficient of variance of indicated mean effective pressure	Exhaust temperatures, °C
0	343.5	24.83	1.565	495
20	328.3	26.00	1.28	492
40	325.2	26.23	0.88	487

stoichiometry) needed to protect engine hardware from excessive temperatures (6).

3.2 Emissions Upstream the Catalysts

3.2.1 Regulated Gaseous Emissions

The exhaust gas emissions from the combustion of gasoline and dual-fuel are detailed in **Figure 3**. The combustion of dual-fuel resulted in different emission trends depending on the composition of methane in the fuel blend. There was a significant reduction in carbon monoxide emissions by 30% and 54% with M20 and M40, respectively, compared to the baseline gasoline mode. In addition, lower CO_2 emissions were observed, mainly due to the simpler chemical structure of methane and its lower carbon content compared to gasoline.

With increased proportion of methane, lower unburned NMHC emissions were produced compared to the gasoline mode. The more homogenous air-fuel mixture of the dual-fuel mode resulted in a more complete combustion and a subsequent reduction in unburnt fuel (11), evident by the increase in CO_2 and H_2O concentrations. Moreover, the decrease in the direct injection of gasoline fuel reduced the liquid fuel impingement into the cylinder walls, reducing wall quenching and resulting in lower carbon monoxide, CO_2 and NMHC emissions.

Conversely, engine-out methane emissions exhibited a contrasting trend to NMHC and CO_2 emissions. With the increase in methane fuel utilisation, methane emissions increased by up to 500 ppm with M40, mainly due to non-combusted methane escaping the combustion chamber. The high global warming potential of methane (30 times greater than CO_2 over a 100 year time frame) may offset the benefits attained by methane utilisation when taking the CO_2-equivalent emissions into consideration. This makes it essential for the development of an efficient aftertreatment system that can efficiently oxidise methane in the dual-fuel system in order to maximise the potential of this strategy (to be discussed further in Section 3.3). On the other hand, nitric oxide emissions increased slightly. This is attributed to the improvement in fuel combustion and the higher adiabatic flame temperature of methane which increases the in-cylinder temperature of the engine at the end

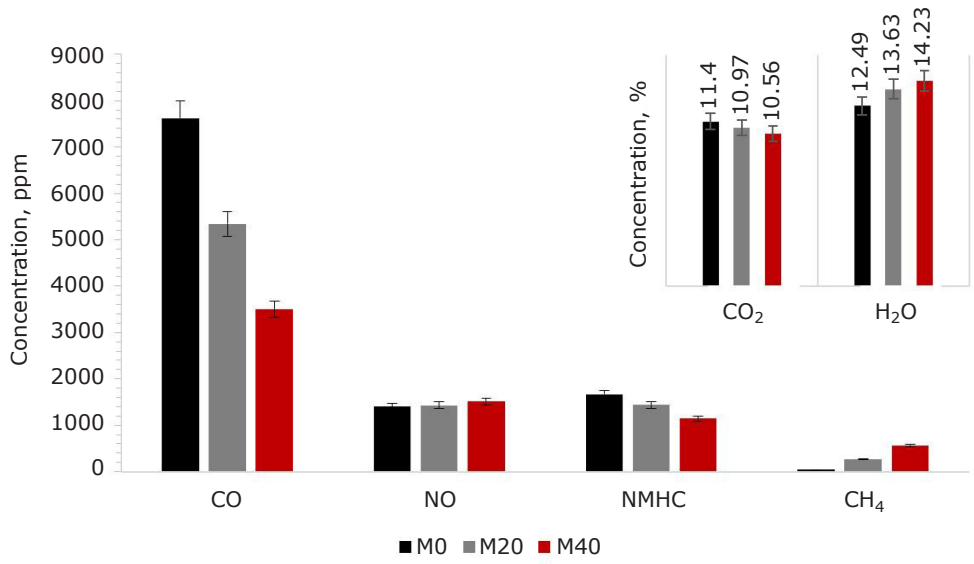

Fig. 3. Engine-out emissions with different methane percentage replacement

of the compression stroke, thus promoting nitric oxide formation (11).

3.2.2 Particulate Matter Emissions

The effect of increasing methane fuel replacement on the particle number distribution of the GDI engine is illustrated in **Figure 4**. The addition of methane gas to the combustion chamber caused a significant reduction in peak particle concentration compared to the base gasoline mode, with 78% reduction observed for M40. This can be directly related to the reduction in aromatic content of the fuel mixture with the addition of methane. The aromatics in gasoline are heavily linked to the initial formation of particles in direct injection engines and the condensation and adsorption that cause the later growth (12). Unlike gasoline, methane's atomic structure does not contain C–C bonds, thereby significantly lowering the formation of soot precursor species such as aromatic HCs and polyaromatic hydrocarbons (13, 14). Moreover, the addition of the gaseous fuel coupled with the reduction of the direct-injected gasoline fuel leads to better mixing and more homogenous combustion. This in turn reduced the fuel-rich areas in which the carbonaceous primary particles are formed and hence, the availability of these particles to undergo pyrolysis reactions (15).

3.3 Impact of Platinum Group Metal Ratio and Methane Replacement on Catalytic Activity

3.3.1 Regulated Gaseous Emissions

The catalyst light-off profiles for gaseous emissions for both the M0 and M40 engine fuelling conditions are shown in **Figure 5**. M20 was not studied in this set of experiments. Light-off tests were carried out using low (L), medium (M) and high (H) pgm catalysts with loadings of 50 g ft^{-3}, 150 g ft^{-3} and 200 g ft^{-3} respectively.

In a TWC, hydrogen and carbon monoxide act as the reducing agents of nitric oxide with selectivity being temperature dependent (16, 17). Two nitric oxide conversion windows were observed across the catalysts for M0 fuelling condition. Firstly, at low temperatures (<200°C) favouring the reduction of nitric oxide by H_2, which reacts with the adsorbed oxygen atoms to produce nitrous oxide (17). Then at temperatures (>200°C), another reduction pathway takes place through reactions with carbon monoxide with the selectivity of hydrogen towards nitric oxide decreasing as it is oxidised by O_2. The same reactions also occur with M40 fuelling. However, an additional nitric oxide conversion window was observed in this case. At higher temperatures (>240°C), the catalysts demonstrated a slower nitric oxide conversion rate with M40 compared to M0. This is attributed to the

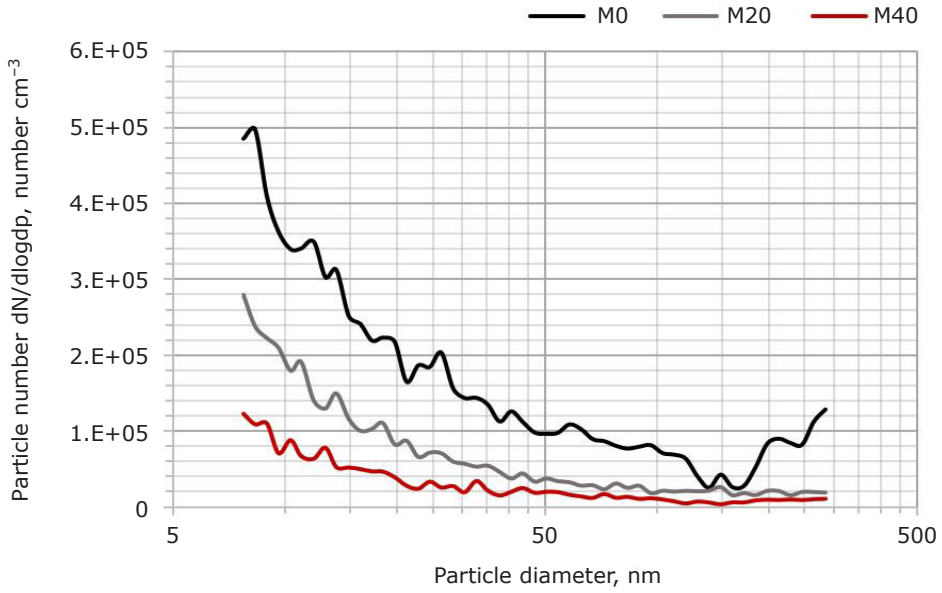

Fig. 4. Particle size distributions

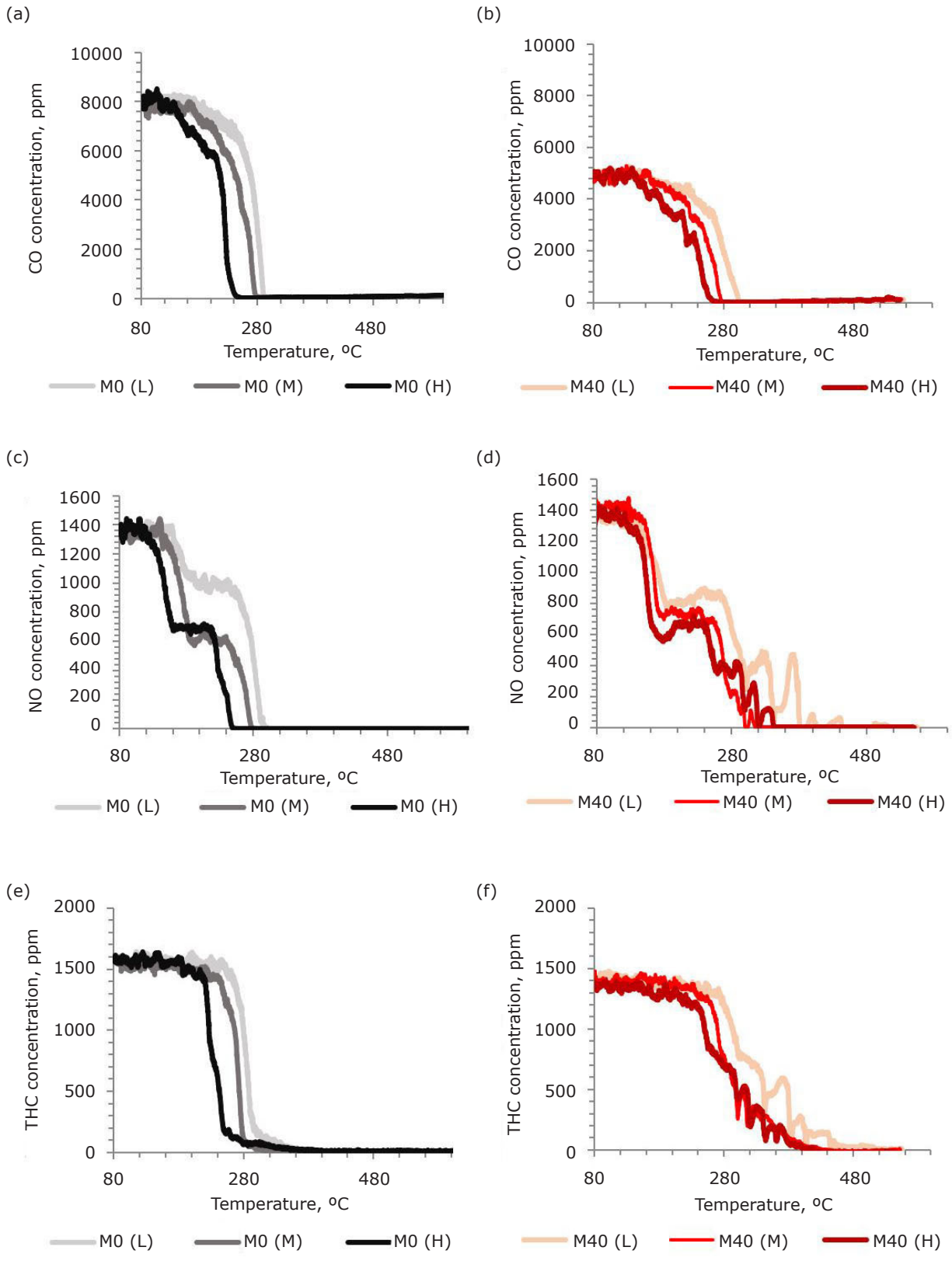

Fig. 5. Catalyst light-off activity for regulated emissions for M0 and M40: (a) carbon monoxide concentration for M0; (b) carbon monoxide concentration for M40; (c) nitric oxide concentration for M0; (d) nitric oxide concentration for M40; (e) THC concentration for M0; (f) THC concentration for M40

lower concentration of carbon monoxide available from engine combustion to participate in nitric oxide reduction with the M40 fuelling, which is the governing reaction pathway at these temperatures. The ratios of the exhaust reductant and oxidant species are key for catalytic reactions in a TWC, and a balance is therefore needed for its efficient operation. As shown in **Figure 5** for the M40 case, carbon monoxide emissions are completely oxidised. However, there is still approximately 350 ppm of nitric oxide present in the exhaust. This excess nitric oxide then reacts with another reducing agent, methane, which has a similar role to carbon monoxide in removing the oxygen from nitric oxide dissociated on the palladium sites (17–19).

On the other hand, light-off catalyst temperatures for THC were significantly delayed with M40 compared to M0, which is attributed to the higher concentrations of methane present in the exhaust gas. Methane constitutes approximately half of the THC concentration in the M40 exhaust and is the most difficult HC to oxidise, thereby shifting the light-off to higher temperatures (see Section 3.2.1).

The effect of increasing the catalyst pgm loading on the regulated emissions light-off temperature is shown in **Figure 6**. Catalysts with higher pgm demonstrated a faster conversion rate than lower pgm catalysts. Carbon monoxide, nitric oxide and THC light-offs were enhanced by approximately 50°C, 110°C and 50°C respectively when using the highest pgm catalyst. This indicates that nitric oxide is significantly more sensitive to pgm loading, specifically rhodium, than other exhaust emissions. The difference in $T_{50\%}$ of nitric oxide between the catalysts with 200 g ft^{-3} and 150 g ft^{-3} loading was significantly lower than the catalyst with loading of 50 g ft^{-3}, indicating that although increasing the rhodium loading has a positive effect on the low-temperature activity of the catalyst, the benefit seems to diminish at pgm >150 g ft^{-3}. Noble metals are known to be expensive, with rhodium being five to six times more costly than palladium and platinum (20), therefore careful economic consideration has to be taken into the optimisation of these noble metal catalyst to reduce the cost while still attaining a relatively fast light-off temperature.

3.3.2 Methane Light-off Study

Figure 7 demonstrates the light-off profile of methane for M0 and M40 respectively. Comparing the two fuelling conditions, there are insignificant differences between methane light-off temperatures for M0 and M40 as both curves superimpose perfectly, despite the significantly higher methane concentration present in the engine exhaust with M40 fuelling. This indicates that the catalyst's ability to oxidise methane is more dependent on temperature rather than fuel composition, i.e. regardless of the concentration of methane flowing through. Moreover, methane conversion starts right after carbon monoxide depletion through a reaction with nitric oxide, as explained in the previous section. Some studies have shown that carbon monoxide acts as an inhibitor for methane conversion, which was also observed in this study (17).

It is well accepted that among pgms, palladium has the greatest effect on the conversion of

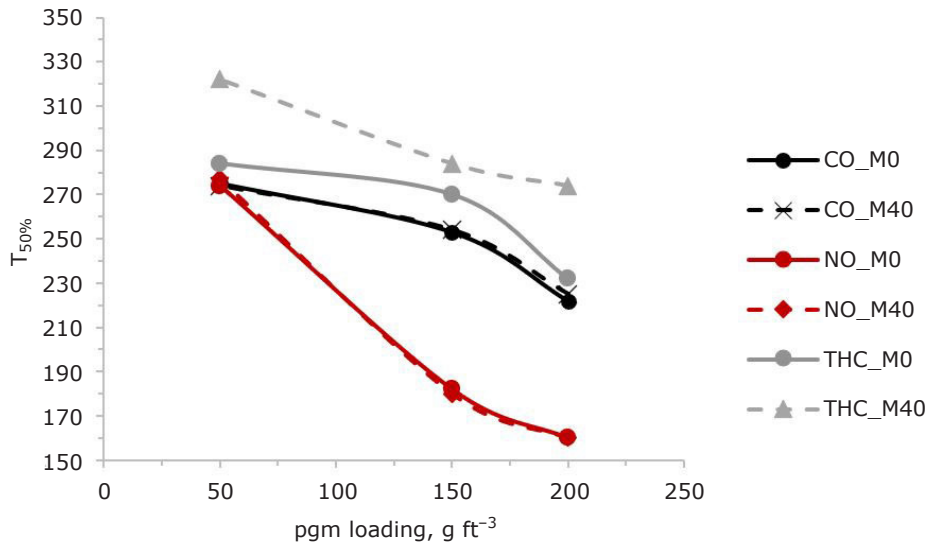

Fig. 6. Regulated emissions light-off temperature *vs*. pgm loading

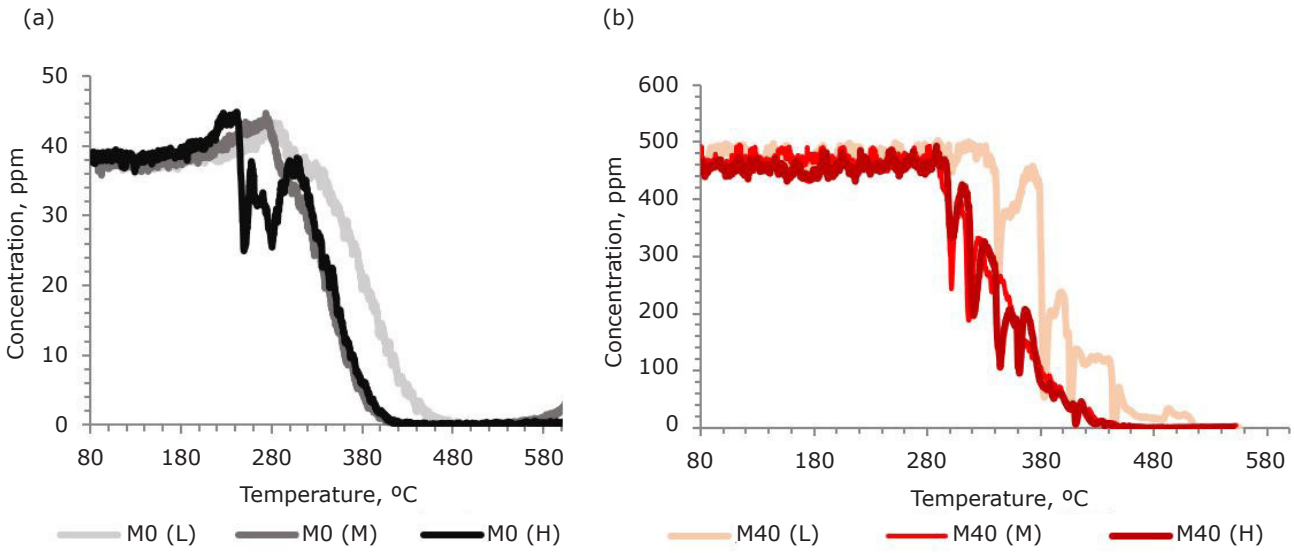

Fig. 7. Light-off activity of methane for: (a) M0; and (b) M40 at different pgm loadings

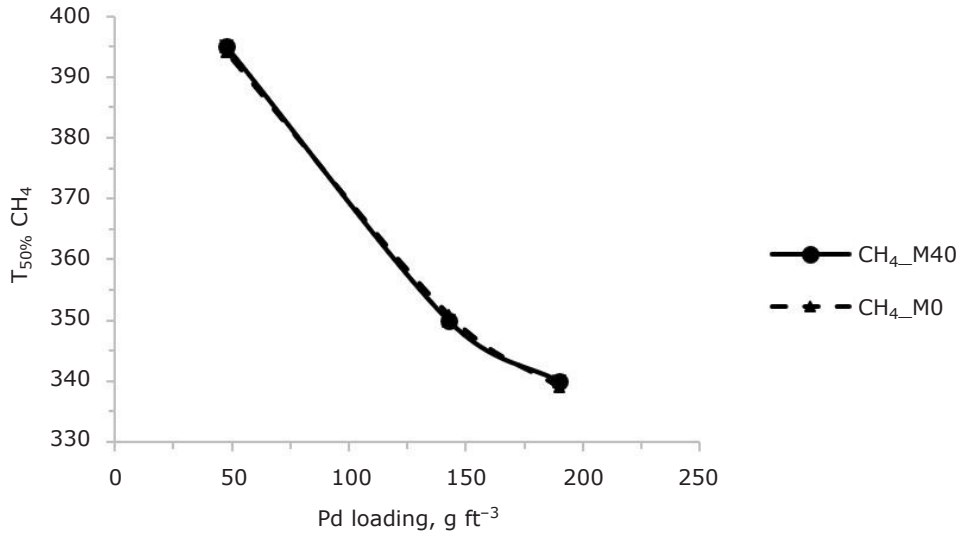

Fig. 8. Methane light-off temperature *vs.* palladium loading

methane, followed by platinum and rhodium (20–22). Generally, the active phase for methane oxidation is known to be PdO (17, 23); however under stoichiometric natural gas vehicle exhaust gas conditions, metallic palladium is the predominant active species (23). The reactivity of metallic palladium is controlled by the competitive adsorption of methane and oxygen at the surface in a Langmuir–Hinshelwood mechanism (18). Hence, in order to oxidise the highly stable methane bond at lower temperatures, the use of palladium loading is essential in the aftertreatment system.

The results shown in **Figure 8** indicate that increasing the palladium loading led to significantly earlier light-off temperatures for methane for both fuelling conditions. Methane light-off temperature for both fuelling conditions was in the order of approximately 340°C, 350°C and 395°C for high, medium and low pgms, respectively. However, the benefit diminished above palladium loading >142.5 g ft^{-3} which suggests that the effect of palladium on methane conversion had reached a plateau, as shown in **Figure 8**. These results are promising compared to other catalyst formulations reported in the literature (22). A point to note is that the high efficiency of palladium is only activated within a quite narrow operating window due to its sensitivity towards oxygen (23). This makes

the control of air-fuel ratio for stoichiometric dual-fuel gasoline engines vital for the efficient operation of its aftertreatment system.

3.3.3 Catalyst Impact on Non-Methane Hydrocarbons

HC reactivity is governed by the respective molecular structure and carbon numbers. It is well documented that short-chain HCs have lower oxidation activity as they require higher energy to detach their stable C–H bond as opposed to longer chain HCs. The oxidative reactivity decreases in the following order: alcohols > aromatics > alkynes > alkenes > alkanes (24, 25). **Figure 9** demonstrates the pre-catalyst concentrations of NMHC for both M0 and M40 case. In general, less NMHCs resulted from M40 combustion.

Propane is the highest NMHC produced with over 225 ppm present in M0 and 125 ppm in M40, followed by ethylene (70 ppm, 45 ppm) and toluene (70 ppm, 30 ppm). Small concentrations of oxygenated HCs acetaldehyde and formaldehyde were found pre-catalyst but were completely oxidised at temperatures <300°C. These species are harmful to humans and are classified as carcinogenic so their aftertreatment control is vital. Some HCs are known to inhibit the oxidation of carbon monoxide and reduction of nitric oxide over a TWC by occupying the catalyst active sites (20, 24). Traces of propylene (also known as propene) were found in the engine exhaust, approximately 40 ppm for M0 and 20 ppm for M40. It has been reported that propylene has a promoting effect on nitric oxide reduction over a palladium-rhodium catalyst (20) which could explain the inferior oxidation activity of nitric oxide for M40.

The light-off temperatures of most HCs were slightly delayed in the M40 fuelling compared to M0 with propane being the HC most affected. The oxygen concentration from the dual-fuel mode was lower compared to the gasoline mode as more oxygen is consumed in the combustion phase to oxidise the injected methane. This resulted in lower concentrations of O_2 that can undergo HC oxidation reactions over the catalyst. On the other hand, increasing the pgm loading led to faster light-off temperatures for all the NMHC species in both fuelling conditions.

3.3.4 Ammonia and Nitrous Oxide Formation Over Compressed Natural Gas Catalyst

Several studies conducted on gasoline-natural gas engines have shown that TWCs are the main cause of high levels of tailpipe ammonia emissions (26, 27). Moreover, the level of ammonia is highly impacted by the operating conditions and air:fuel ratio with the highest level occurring during rich driving conditions. The formation of ammonia depends on the kinetic behaviour and chain effect of the different reductant and oxidant species in the exhaust and their interaction over the TWC as shown through Equations (i)–(iv) (17, 20, 26–29):

$$2NO + 5H_2 \rightarrow 2NH_3 + 2H_2O \quad \text{(i)}$$

$$2NO + 2CO + 3H_2 \rightarrow 2NH_3 + 2CO_2 \quad \text{(ii)}$$

$$2NO + H_2 \rightarrow N_2O + H_2O \quad \text{(iii)}$$

$$2NH_3 + 4NO \rightarrow N_2O + 3H_2O + 2N_2 \quad \text{(iv)}$$

Figure 10 displays the ammonia formation over the CNG catalysts for the different pgm loadings and fuelling conditions along with levels of hydrogen, nitric oxide and nitrous oxide, the byproducts of ammonia formation and oxidation. Ammonia is formed over the catalyst *via* the reaction of nitric oxide with hydrogen (Equation (i)), whereby the hydrogen atoms remove the oxygen atoms from the dissociation of nitric oxide before further reacting with the nitrogen atoms (27, 28, 30). An alternate reaction pathway can occur *via* further reaction with carbon monoxide (Equation (ii)), which helps in ammonia formation through its participation in the removal of oxygen atoms, thereby facilitating the direct reaction of hydrogen atoms with nitrogen atoms and also through the intermediate hydrolysis of isocyanic acid (29). However, nitric oxide reduction can also lead to another pathway forming nitrous oxide instead, with the selectivity depending on temperature and the kinetic reactions of the different species. As demonstrated in **Figure 10**, initially nitric oxide reacts with hydrogen at approximately 100°C to form nitrous oxide (Equation (iii)). The selectivity of the catalyst then changes momentarily to form ammonia within a narrow temperature window 180–280°C before changing back again to nitrous oxide. This indicates that the selectivity of the catalyst towards ammonia formation at low temperatures occurs only within a narrow temperature window provided that enough hydrogen is available to undergo nitric oxide reduction. Ammonia levels then reduce either through oxidation by oxygen or through ammonia decomposition *via* Equation (iv) (29).

Considering the M0 fuelling condition at high temperatures (>300°C), ammonia concentration

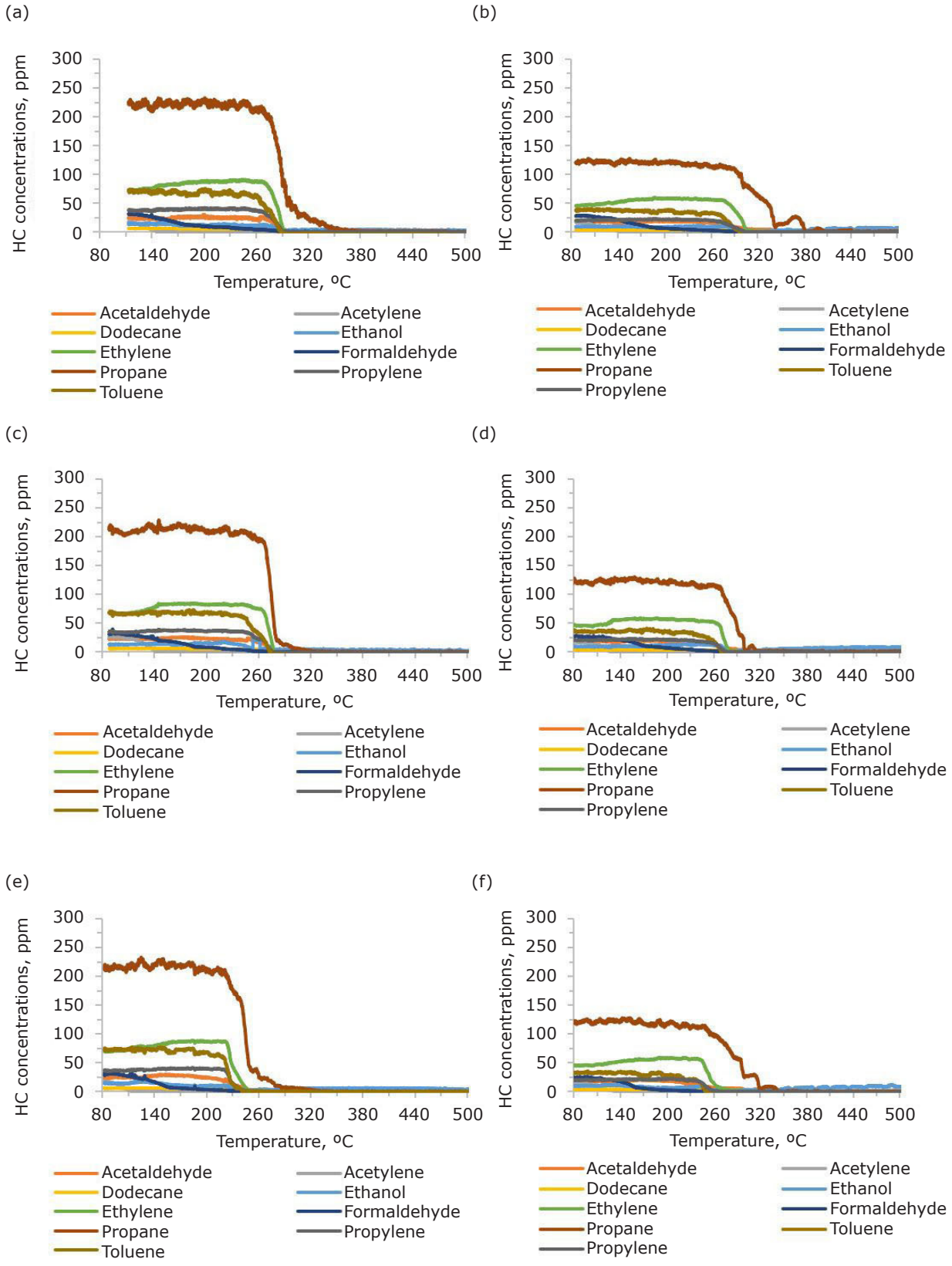

Fig. 9. NMHC light-off activity for M0 and M40: (a) high pgm M0; (b) high pgm M40; (c) medium pgm M0; (d) medium pgm M40; (e) low pgm M0; (f) low pgm M40

stabilises following a sharp decrease. This is attributed to water gas shift (WGS) reactions (Equation (v)) which increases the availability of hydrogen to take part in ammonia formation *via* (Equation (i)). With further increase in temperature, the amount of hydrogen reduces

due to the more favourable reactions with oxygen and the WGS equilibrium constraint at higher temperatures (29). This subsequently reduces the ammonia concentration gradually to 25 ppm as observed in **Figure 10**. Conversely, for the M40 fuelling condition higher ammonia levels are

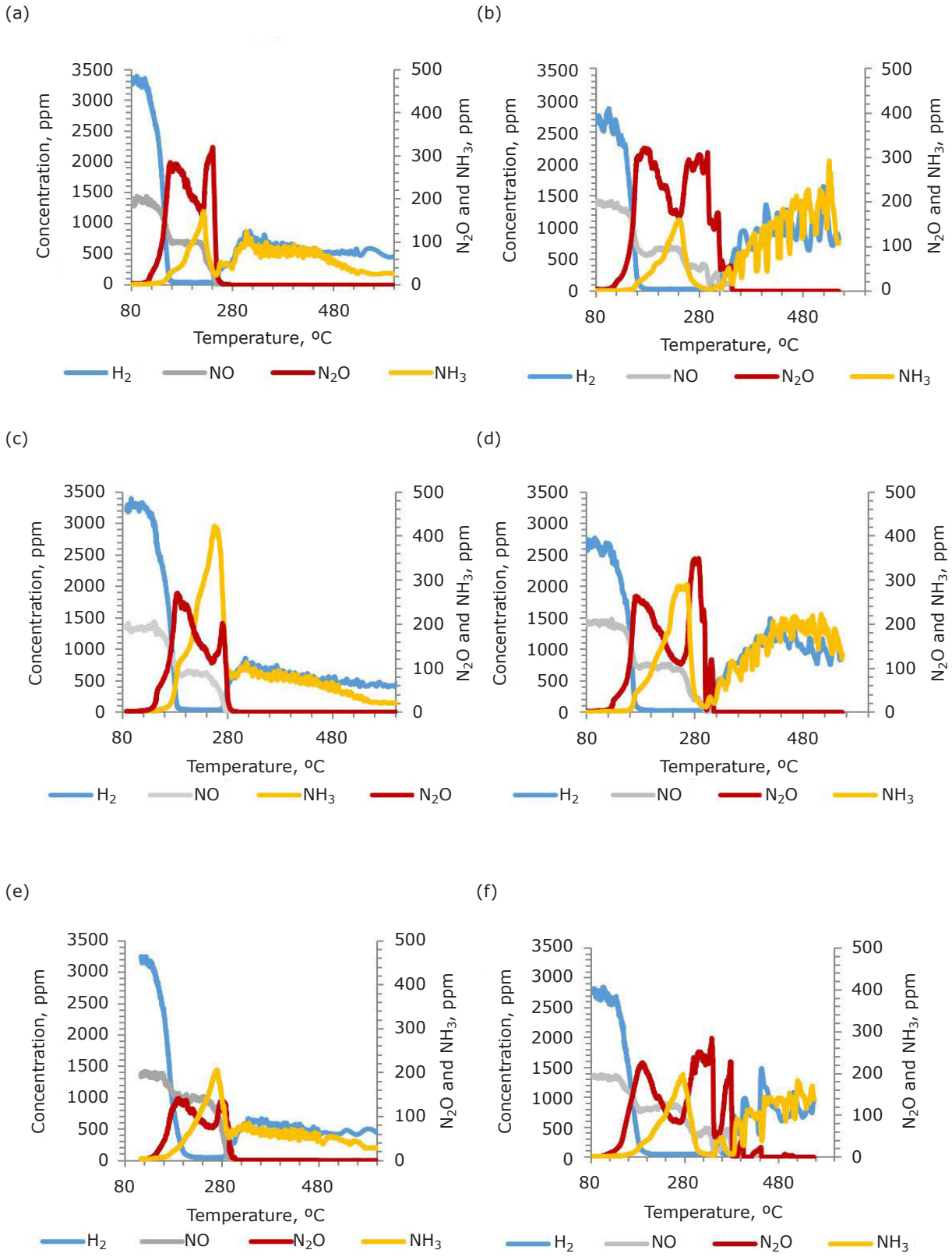

Fig. 10. Ammonia slippage and byproducts for M0 and M40: (a) high pgm M0; (b) high pgm M40; (c) medium pgm M0; (d) medium pgm M40; (e) low pgm M0; (f) low pgm M40

seen at high temperatures with concentrations stabilising at 150–200 ppm. Apart from the WGS reactions, the higher levels of methane in the exhaust stream resulted from M40 combustion mean more methane was available to undergo steam-reforming reactions (Equation (vi)), thereby producing higher hydrogen concentrations as shown in **Figure 10**. This additional hydrogen increases the formation of ammonia in the high temperature region (>300°C). The high level of ammonia slippage in the dual-fuel mode presents a challenge due to the health risks these emissions impose and hence aftertreatment SCR technology should be adopted to remove them.

$$CO + H_2O \rightarrow CO_2 + H_2 \quad (v)$$

$$CH_4 + H_2O \rightarrow CO + 3H_2 \quad (vi)$$

For both fuels, an ammonia peak was observed at different low temperatures (<300°C) depending on the pgm content with reactivity following the order: high pgm > medium pgm > low pgm. The peak concentration of ammonia differs across the three catalysts with the highest concentration produced across the medium pgm catalyst (400 ppm) followed by low pgm (200 ppm). In contrast, high pgm resulted in the lowest peak level of ammonia (150 ppm). Comparing the effect of pgm content at high temperatures (>300°C), there is no difference between the activities of the three catalysts, with all three curves superimposing each other. Hence, the effect of pgm loading on ammonia is only apparent at low temperatures.

4. Conclusions

The potential of a dual-fuel methane-gasoline strategy mode on the performance of a SI gasoline engine and the efficiency of novel CNG catalysts was investigated. The study has effectively addressed one of the major challenges of the dual-fuel system reported in the literature: the tailpipe methane emissions. The different pgm loaded CNG catalysts effectively reduced the engine-out exhaust emissions, especially the higher concentration of methane from the dual-fuel combustion at relatively lower temperatures. The light-off temperature for methane was achieved at 340°C, 350°C and 395°C for high, medium and low pgms respectively. However, another challenge was identified in the study that resulted from the dual-fuel mode. High concentrations of ammonia emissions were produced over the catalyst, which were primarily formed from steam-reforming reactions due to the increased level of methane in the exhaust stream. Therefore, further research into dual-fuel strategy development coupled with SCR technology should be conducted in the future to deal with these harmful ammonia emissions. The results from the study further demonstrated that the dual injection mode can achieve improvements in terms of better fuel economy, lower NMHC, carbon monoxide and CO_2 emissions compared to the GDI mode. This is attributed to the more homogenous mixture and complete combustion with the introduction of the gaseous fuel. In addition, the lower carbon:hydrogen ratio resulted in significantly lower PM emissions.

References

1. H. M. Cho and B.-Q. He, *Energy Convers. Manag.*, 2007, **48**, (2), 608
2. T. Korakianitis, A. M. Namasivayam and R. J. Crookes, *Prog. Energy Combust. Sci.*, 2011, **37**, (1), 89
3. A. Wahbi, A. Tsolakis and J. Herreros, 'Emissions Control Technologies for Natural Gas Engines', in "Natural Gas Engines: For Transportation and Power Generation", eds. K. K. Srinivasan, A. K. Agarwal, S. R. Krishnan and V. Mulone, Energy, Environment and Sustainability Series, Springer Nature Singapore Pte, Singapore, 2019, pp. 359–379
4. A. R. Tabar, A. A. Hamidi and H. Ghadamian, *Int. J. Energy Environ. Eng.*, 2017, **8**, (1), 37
5. J. Obiols, D. Soleri, N. Dioc and M. Moreau, SAE Technical Paper 2011-01-1995, SAE International, Warrendale, USA, 30th August, 2011
6. E. Singh, K. Morganti and R. Dibble, *Fuel*, 2019, **237**, 694
7. Z. Chen, L. Wang and K. Zeng, *Energy Convers. Manag.*, 2019, **192**, 11
8. Y. Xu, Y. Zhang, J. Gong, S. Su and Z. Wei, *Fuel*, 2020, **266**, 116957
9. K. Lehtoranta, T. Murtonen, H. Vesala, P. Koponen, J. Alanen, P. Simonen, T. Rönkkö, H. Timonen, S. Saarikoski, T. Maunula, K. Kallinen and S. Korhonen, *Emiss. Control Sci. Technol.*, 2017, **3**, (2), 142
10. A. Raj, *Johnson Matthey Technol. Rev.*, 2016, **60**, (4), 228
11. H. Chen, J. He and X. Zhong, *J. Energy Inst.*, 2019, **92**, (4), 1123
12. D. R. Tree and K. I. Svensson, *Prog. Energy Combust. Sci.*, 2007, **33**, (3), 272
13. G. Karavalakis, T. D. Durbin, M. Villela and J. W. Miller, *J. Nat. Gas Sci. Eng.*, 2012, **4**, 8

14. J. Alanen, E. Saukko, K. Lehtoranta, T. Murtonen, H. Timonen, R. Hillamo, P. Karjalainen, H. Kuuluvainen, J. Harra, J. Keskinen and T. Rönkkö, *Fuel*, 2015, **162**, 155
15. K. Nithyanandan, Y. Lin, R. Donahue, X. Meng, J. Zhang and C. Lee, *Fuel*, 2016, **184**, 145
16. F. Dhainaut, S. Pietrzyk and P. Granger, *Catal. Today*, 2007, **119**, (1–4), 94
17. M. Salaün, A. Kouakou, S. Da Costa and P. Da Costa, *Appl. Catal. B: Environ.*, 2009, **88**, (3–4), 386
18. M. Monai, T. Montini, R. J. Gorte and P. Fornasiero, *Eur. J. Inorg. Chem.*, 2018, (25), 2884
19. R. Marques, S. Capela, S. Da Costa, F. Delacroix, G. Djéga-Mariadassou and P. Da Costa, *Catal. Commun.*, 2008, **9**, (8), 1704
20. Y. Ren, D. Lou, P. Tan, Y. Zhang and X. Sun, *J. Clean. Prod.*, 2021, **298**, 126833
21. T. Sakai, B.–C. Choi, R. Osuga and Y. Ko, 'Purification Characteristics of Catalytic Converters for Natural Gas Fueled Automotive Engine', SAE Technical Paper No. 912599, SAE International, Warrendale, USA, 1991
22. S. Trivedi, R. Prasad, A. Mishra, A. Kalam and P. Yadav, *Environ. Sci. Pollut. Res.*, 2020, **27**, (32), 39977
23. J. Chen, Y. Wu, W. Hu, P. Qu, G. Zhang, Y. Jiao, L. Zhong and Y. Chen, *Ind. Eng. Chem. Res.*, 2019, **58**, (16), 6255
24. M. Bogarra, J. M. Herreros, C. Hergueta, A. Tsolakis, A. P. E. York and P. J. Millington, *Johnson Matthey Technol. Rev.*, 2017, **61**, (4), 329
25. A. O. Rusu and E. Dumitriu, *Environ. Eng. Manag. J.*, 2003, **2**, (4), 273
26. S. Pradhan, A. Thiruvengadam, P. Thiruvengadam, B. Demirgok, M. Besch, D. Carder and B. Sathiamoorthy, *SAE Int. J. Engines*, 2017, **10**, (1), 104
27. Q. Zhang, M. Li, S. Shao and G. Li, *Appl. Therm. Eng.*, 2018, **130**, 1363
28. R. Suarez-Bertoa, A. A. Zardini and C. Astorga, *Atmos. Environ.*, 2014, **97**, 43
29. S. H. Oh and T. Triplett, *Catal. Today*, 2014, **231**, 22
30. K. Ramanathan, C. S. Sharma and C. H. Kim, *Ind. Eng. Chem. Res.*, 2012, **51**, (3), 1198

The Authors

Ammar Wahbi obtained his PhD degree at the University of Birmingham, UK, in 2022 and has since moved to industry working in the development and calibration of flagship gasoline engines. His PhD research was sponsored by Johnson Matthey and focused on gasoline-methane dual-fuel injection performance and the development of its after-treatment system. His work involved physiochemical characterisation of gasoline direct injection soot, performance of gasoline particulate filters and gasoline fuel reforming to improve fuel efficiency and pollutant control. He also worked in the development of diesel emissions control systems including hydrocarbon-selective catalytic reduction and methane-slip catalyst for lean burn conditions.

Professor Athanasios Tsolakis has academic and industrial expertise in the field of low carbon energy carriers, environmental catalysts, combustion and pollutant control technologies. Prior to his academic appointment at the University of Birmingham in 2005 he worked as a research scientist at Johnson Matthey. In 2009 he was elected Fellow of the Institution of Mechanical Engineers (FIMechE) and in 2011 he was elected Fellow of the Higher Education Academy (FHEA). Since 2015 he is the Director of Research for the School of Engineering at the University of Birmingham.

Jose M. Herreros is an Associate Professor in Vehicle Engineering at the School of Engineering at the University of Birmingham. His research focuses on the investigation of clean and efficient powertrain systems based on the energy and emissions efficient integration of various propulsion systems with the ultimate goal to develop energy-efficient and clean powertrains to be used in vehicular applications. He has published journal articles on issues related to fuel design and properties, pollutant emissions characterisation and catalysis.

Omid Doustdar is an Assistant Professor in the Department of Mechanical Engineering, School of Engineering at the University of Birmingham. He obtained MEng degree in Mechanical Engineering in 2012 and PhD in 2019 from the University of Birmingham under the supervision of Professor Athanasios Tsolakis and Professor Miroslaw Wyszynski. He has more than ten years of teaching, research and industrial experience in environmental pollutants control and decarbonisation technologies, working as a research fellow and a teaching fellow at the University of Birmingham and working as a seconded researcher in world-leading industries and collaborating with them in power solution, marine and transportation.

Soheil Zeraati Rezaei is a lecturer in Clean Energy Engineering at the School of Engineering, University of Birmingham. His research and publications have mainly focused on alternative energy carriers and conversion for transportation and power systems, environmental pollutants characterisation and control.

Paul Millington originally joined Johnson Matthey in the Emission Control Research group in 1995. After a short break in the automotive industry he rejoined in 2001. He currently works on all forms of pgm-containing aftertreatment in the Emission Control Research group at Johnson Matthey.

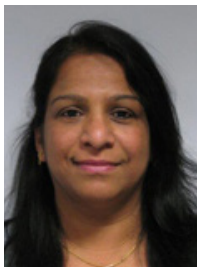

Agnes Raj joined Johnson Matthey in 2007. She obtained her MSc and MPhil in Chemistry from the University of Madras, India, and PhD in Material Science from Imperial College London, UK. She has strong technical experience in research and development activities focused on catalysts applicable for diesel and compressed natural gas aftertreatment systems.